Biochimica et Biophysica Acta 1863 (2017) 1002–1012

Contents lists available at ScienceDirect

Biochimica et Biophysica Acta

journal homepage: www.elsevier.com/locate/bbadis

UCP2 up-regulation within the course of autoimmune encephalomyelitis correlates with T-lymphocyte activation

Alina Smorodchenko [a,b,*], Stephanie Schneider [a], Anne Rupprecht [a], Karoline Hilse [a], Soleman Sasgary [a], Ute Zeitz [a], Reinhold G. Erben [a], Elena E. Pohl [a,**]

[a] Institute of Physiology, Pathophysiology and Biophysics, University of Veterinary Medicine, Vienna, Austria
[b] Institute of Vegetative Anatomy, Charité — Universitätsmedizin Berlin, Germany

ARTICLE INFO

Article history:
Received 9 October 2016
Received in revised form 7 January 2017
Accepted 23 January 2017
Available online 25 January 2017

Keywords:
Neuroinflammation
Mitochondrial uncoupling proteins
Central nervous system
Metabolic re-programming of cells
Cell proliferation
UCP4

ABSTRACT

Multiple sclerosis (MS) is an inflammatory demyelinating autoimmune disorder of the central nervous system (CNS) associated with severe neurological disability. Reactive oxygen species (ROS) and mitochondrial dysfunction play a pivotal role in the pathogenesis of this disease. Several members of the mitochondrial uncoupling protein subfamily (UCP2–UCP5) were suggested to regulate ROS by diminishing the mitochondrial membrane potential and constitute therefore a promising pharmacological target for MS. To evaluate the role of different uncoupling proteins in neuroinflammation, we have investigated their expression patterns in murine brain and spinal cord (SC) during different stages of experimental autoimmune encephalomyelitis (EAE), an animal model for MS. At mRNA and protein levels we found that only UCP2 is up-regulated in the SC, but not in brain. The increase in UCP2 expression was antigen-independent, reached its maximum between 14 and 21 days in both OVA and MOG immunized animals and correlated with an augmented number of $CD3^+$ T-lymphocytes in SC parenchyma. The decrease in abundance of UCP4 was due to neuronal injury and was only detected in CNS of MOG-induced EAE animals. The results provide evidence that the involvement of mitochondrial UCP2 in CNS inflammation during EAE may be mainly explained by the invasion of activated T-lymphocytes. This conclusion coincides with our previous observation that UCP2 is up-regulated in activated and rapidly proliferating T-cells and participates in fast metabolic re-programming of cells during proliferation.

1. Introduction

Multiple sclerosis (MS) and its animal model – experimental autoimmune encephalomyelitis (EAE) – are T-cell-mediated inflammatory and demyelinating autoimmune diseases of the central nervous system (CNS) associated with severe neurological disability [1,2]. The molecular mechanisms leading to the histopathological hallmarks of MS are still ambiguous. Increasing evidence shows that oxidative stress and mitochondrial injury play an important role in MS pathogenesis by contributing to lesion formation [3–5]. Activated macrophages and resident microglia in acute inflammatory lesions are suggested to be the main source of pro-inflammatory cytokines and ROS production [6].

Excessive ROS production in mitochondria is attributed to respiratory chain function. Decreasing the proton motive force by mild uncoupling was proposed to be an effective way to diminish ROS [7]. Uncoupling proteins (UCP2–5) belong to the mitochondrial anion transporter superfamily and have been controversially discussed for years for involvement in ROS regulation by decreasing the proton gradient through the inner mitochondrial membrane (for review [8]), although evidence for their role in metabolism permanently increases [9,10]. In the context of ROS regulation, UCP2 was proposed to be involved in the pathogenesis of neurodegenerative and neuroinflammatory diseases, in particular in MS or EAE [11–15]. The main arguments for UCP2's protective role were the up-regulation of UCP2 gene expression in the inflamed spinal cord of EAE mice [16] and higher clinical scores of the disease in UCP2 knockout mice [13]. No clear picture concerning the

Abbreviations: AB, antibody; BSA, bovine serum albumin; COX, Cytochrom c Oxidase (Complex IV); CFA, complete Freund adjuvant; dpi, day post injection; CNS, central nervous system; DAB, 3,3`-diaminobenzidine tetrahydrochloride; EAE, experimental autoimmune encephalomyelitis; GFAP, glial fibrillary acidic protein; IBA, ionized calcium binding adaptor molecule; IHC, immunohistochemistry; HRP, horse radish peroxidase; Hsp60, heat shock protein 60; MHC, major histocompatibility complex; MOG, myelin oligodendrocyte protein; MS, multiple sclerosis; NGS, normal goat serum; OVA, ovalbumin; OT-II cells, ovalbumin peptide specific T-cells; PBS, phosphate buffer saline; PCR, polymerase chain reaction; PFA, paraformaldehyde; ROS, reactive oxygen species; SC, spinal cord; SEM, standard error of the mean; SOD2, superoxide dismutase 2; VDAC, voltage dependent anion channel; UCP, uncoupling protein; WB, Western Blot.

* Correspondence to: Alina Smorodchenko, Institute of Vegetative Anatomy, Charite-Universitätsklinikum Berlin, Germany.
** Correspondence to: Elena E. Pohl, Institute of Physiology, Pathophysiology and Biophysics, University of Veterinary Medicine, Vienna, Austria.
E-mail addresses: alina.smorodchenko@charite.de (A. Smorodchenko), elena.pohl@vetmeduni.ac.at (E.E. Pohl).

http://dx.doi.org/10.1016/j.bbadis.2017.01.019
0925-4439/

type of cells which up-regulate UCP2 during MS/EAE has emerged from previous studies. Recently we demonstrated that only UCP4 is present in neurons and neurosensory cells at physiological conditions [9,17,18]. We found UCP2 in cells of the immune system including brain microglia confirming previous reports [19,20]. The UCP2 expression pattern implies strong involvement in the metabolism of highly proliferating and/or activated cells [9].

In the present work we aimed to test the hypothesis that the up-regulation of UCP2 occurs due to invasion of activated T-cells in CNS during inflammation and not due to protein overexpression in neurons. For this we compared (i) mRNA and protein levels of UCP2, UCP4 and UCP5 at different EAE stages (early, acute and chronic), (ii) the expression of UCP2 after immunization with non-neural OVA-protein, (iii) expression of the respective hallmarks for autoimmune damage (neuronal injury, axonal loss, reactive astro- and microgliosis) and (iv) the number of $CD3^+$ T-lymphocytes at different stages of CNS-unspecific (OVA) and specific (MOG) immunization.

2. Methods

2.1. EAE induction in mice

Female C57BL/6J mice aged 4–6 weeks were obtained from Harlan Laboratories S.r.J. (Italy), maintained in cages and housed for two weeks in accordance with international and university guidelines for animal care. Mice were subcutaneously immunized with 250 μg of myelin oligodendrocyte glycoprotein (MOG) (Pepceuticals Ltd., UK) solved in 200 μl emulsion containing equal volumes of phosphate buffer saline (PBS), CFA (Difco Laboratories Inc, USA) and 4 mg/ml Mycobacterium tuberculosis H37Ra (Difco Laboratories Inc, USA). For the control groups of mice we used the emulsion contained ovalbumin (OVA, Pepceuticals Ltd., UK) instead of MOG which was prepared in the same way. Mice from both groups received an intraperitoneal (i.p.) injection of 400 ng *Bordetella* pertussis toxin (Merck, Austria) at days 0 and 2 after immunization. Mice were weighed daily and scored (Tables 1 and 2) using the five-grade scale, as described previously [21]. In short, we attribute the following scores according to the clinical signs of disease: 0, healthy mouse; 1, weak or flaccid tail; 1.5, limp tail and unsteady gait; 2, unsteady gait (ataxia), hind leg paresis; 2.5, clumsy gait, hind leg paresis (partial dragging); 3, paraparesis of one or two hind limbs; 3.5, paraparesis of one or two hind limbs, forelimb weakness; 4, paraparesis with fore limb involvement; 4.5, paraparesis of hind limbs, paresis of fore limbs (cannot move or groom); 5, moribund or dead.

The animals used in experiments were sacrificed at 5, 14 and 21 days post injection (dpi). In addition to the first control group treated with OVA, a second control group was established, consisting of age-matched, healthy, and not immunized C57BL/6 mice.

All procedures were performed in accordance with prevailing guidelines for animal care, and were approved by the Ethical Committees of the University of Veterinary Medicine and of the Austrian Federal Ministry of Science and Research (Animal experiment authorization: 01/04/97/2010).

Table 1
Clinical scores determined for C57BL/6 mice at 5, 14 and 21 dpi with encephalitogenic (MOG) and non-encephalitogenic peptides (OVA). Clinical scores were determined according grading system for EAE clinical assessment (s. Methods). Not treated (naïve) mice served as a control. Values represent a mean ± SD for n = 10–11 per group.

Group	Dpi, day after injection		
	5	14	21
MOG	0	3.25 ± 0.96	2.1 ± 0.99
OVA	0	0	0
Naive	0	0	0

Table 2
Weight monitoring of C57BL/6 mice at 5, 14 and 21 dpi with encephalitogenic (MOG) and non-encephalitogenic peptides (OVA). Not treated (naïve) mice served as a control littermates. Values represent a mean ± SD for n = 10-11 per group.

Group	Dpi, day after injection			
	0 Initial weight	5	14	21
MOG	18.0 ± 0.87	16.8 ± 1.10	17.0 ± 2.79	17.2 ± 3.31
OVA	18.54 ± 0.79	17.38 ± 1.29	18.77 ± 2.18	19.45 ± 2.11
Naive	18.36 ± 0.50	18.68 ± 0.66	19.47 ± 0.85	20.18 ± 0.73

2.2. Immunohistochemistry (IHC)

Mice were deeply anaesthetized with a mixture containing ketamine (Pfizer, Karlsruhe, Germany) and xylazine (Rompun®, Bayer, Germany), then intracardially perfused with 20 ml ice-cold 0.1 M PBS and 20 ml 4% paraformaldehyde (PFA). Brain and SC were removed and fixed in 4% PFA. For fluorescence microscopy, we used cryo- and vibratom tissue sections. 50 μm thick vibratome sections without cryoprotection were prepared using a Leica VT1000 vibratome (Leica Microsystems, Germany). For cryo-sections organs were incubated in 0.8–1.4 M phosphate-buffered sucrose for 5 days at +4 °C for cryoprotection, than embedded in a tissue-freezing medium obtained from Leica Microsystems GmbH (Germany). The tissues were sectioned (20 μm thick) at −26 °C using Jung Frigocut Cryostat Microtome (Leica, Germany), mounted on Superfrost™ microscope slides (Erie Scientific, Portsmouth NH, USA) and stored at −20 °C until staining. As primary antibodies (AB) for detection of UCP4, MHC class II, microglia, astrocytes and lymphocytes we used rabbit anti-UCP4 (1:1000, [18]), rat anti-rat RT1Bu (1:4; Serotec, UK/International), goat anti-SOD2 (Santa Cruz, 1:50), mouse anti-glial fibrillary acidic protein (GFAP; 1:750; DAKO GmbH, Germany) and rat anti-CD3 antibody (1:100; AbD Serotec, UK). Negative control sections were incubated in a similar manner, except that the primary AB was replaced by normal goat serum (NGS; Vector Laboratories, Burlingame, USA). For visualization of primary ABs, goat anti-rabbit IgG conjugated with Alexa-488 (diluted 1:1000, Invitrogen, Germany) and goat anti-mouse/rat IgG conjugated with Alexa-568 (1:1000, Invitrogen, Germany) were used as secondary ABs.

For light microscopy analysis we used vibratome and paraffin-embedded sections. 8 μm thick paraffin sections were cut using Microm HM 355S (Leica), deparaffinized in xylene and heated in sodium citrate buffer in the microwave to unmask the antigen. The sections were incubated with primary antibodies as described above. As secondary antibodies, biotinylated anti-rat IgG (dilution 1:1000; Linaris GmbH, Wertheim, Germany), anti-mouse IgG (1:1000; Vector Laboratories, Burlingame, USA) and anti-rabbit IgG (1:1000; Vector Laboratories, USA) were used. Finally, sections were pre-incubated with ABC-solution (ABC-Elite; Vector Laboratories, USA) and developed with 0.03% H_2O_2 and 1% 3,3`-diaminobenzidine tetrahydrochloride (DAB, Sigma-Aldrich).

2.3. Luxol Fast Blue staining

The spinal cord sections were stained with Luxol Fast Blue according to the standard protocol [22]. In brief, deparaffinized sections were incubated with Luxol Fast Blue solution (0.1% in 95% alcohol with 0.5% acetic acid) at 57 °C overnight. After short differentiation by quick immersion in lithium carbonate solution (0.05%), the slides were rinsed twice with 70% ethanol, counterstained with hematoxyline, dehydrated in an ethanol series, cleared in xylene, and coverslipped with Entellan (Merck, Darmstadt, Germany).

2.4. Light and confocal microscopy

Digital images of selected sections were taken using an Olympus BX-51 microscope (Hamburg, Germany). Confocal images were acquired in sequential scanning mode using Leica TCS SP5 equipped with a 63x oil-immersion objective. Argon (488 nm) and DPSS (561 nm) lasers were used respectively for the excitation of Alexa-488 and Alexa-568. During the processing stage, individual image channels were pseudo-colored according to the fluorophore emission spectrum. Image J software (http://rsb.info.nih.gov/ij/) was used for image merging, background correction and adjustment of brightness and contrast.

2.5. Western blot analysis (WB)

Protein samples for Western blots (WB) were obtained from the mouse brain, spinal cord, thymus and spleen. Tissues were homogenized in RIPA buffer containing the protease inhibitor cocktail (Sigma-Aldrich, Austria), sonicated and centrifuged at 1000xg for 10 min at 4 °C. Total protein concentrations were determined using Pierce™ BCA Protein Assay Kit (Thermo Scientific, Rockford, USA). 20–100 μg of total protein from brain, spinal cord, thymus and spleen were loaded on 15% SDS-PAGE Gel, followed by a transfer to nitrocellulose membranes (PEQLAB, Austria). After blocking in 2% BSA, membranes were incubated overnight at 4 °C with affinity purified antibodies. The following ABs were used: rabbit anti-UCP2 (1:1000; [19], rabbit anti-UCP4, rabbit anti-UCP5 (1:1000, [17]), rabbit anti-IBA1 (1:1000; Wako Chemicals, Neuss, Germany), mouse anti-GFAP (1:400, DAKO Deutschland GmbH, Germany), mouse anti-Hsp60 (1:10000, Abcam), GAPDH (1:2500, Sigma) and mouse anti-CD3 (1:100; Abcam). Anti-rabbit IgG and anti-mouse IgG coupled to HRP (GE Healthcare, UK) were used as secondary ABs. For visualization of AB binding the chemiluminescence reaction of the ECL™-Prime Western Blotting Detection Reagent (GE Healthcare, Buckighamshire, UK) was used. The membranes were then stripped and sequentially incubated with ABs against VDAC (1:10000; Abcam, Cambridge, UK) and β-actin (1:5000; Sigma-Aldrich, Germany). The production of recombinant UCP2 and UCP5, used as positive controls, was performed as described previously [23,24].

2.6. Quantitative real-time PCR

Frozen spinal cord and brain samples were put into steel cylinders, cooled in liquid nitrogen and then shredded in a Retsch mill 200 (1 min., 30 sec^{-1}; (Retsch GmbH, Germany)). Total RNA was isolated from the brain and spinal cord of naïve, OVA- and MOG immunized animals at day 5 and day 14 dpi using RNeasy Mini Kit from Qiagen (Hilden, Germany) according to the manufacturer's protocol. The total RNA content was determined with the BioPhotometer (Eppendorf, Austria). RNA quality was tested with the BioAnalyzer (Agilent, Austria) using RNA 6000 Nano Kit (Agilent 2100 Bioanalyzer, USA). Reverse transcription was performed with a High-Capacity cDNA Reverse Transcription Kit (Applied Biosystems, Austria) and random primers. Relative quantification of the target genes was done using Qiagen QuantiFast Multiplex PCR Kit at a final volume of 10 μl, with 300 nM of each primer and a 200 nM probe. The gene expression was measured with the Light Cycler 480 (Roche Diagnostics GmbH, Vienna, Austria) using the following program: initial denaturation for 5 min at 95 °C, followed by 45 cycles of 30 s at 95 °C and 50 s at 62 °C. The relative amount of target gene mRNA was normalized to glyceraldehyde-3-phosphate dehydrogenase (GAPDH) gene as an internal standard. Negative controls (without reverse transcriptase) were used for each sample to exclude contamination with genomic DNA. Primers used for the PCR were obtained from (Eurofins, Germany) and were (name, forward, reverse, and probe):

mUcp2-forward: GCTGGTGGTGGTCGGAGATA
mUcp2-reverse: ATGGCATTACGGGCAACATT
mUcp2-son: AGCACTGTCGAAGCCTACAAGACCATTGC
mUcp4-forward: TCTGGACTTGTGGCTTCTATTCTG
mUcp4-reverse: GTTTGTCTCGAGGTTGGTTCATT
mUcp4-son: CCAGCCGATGTCATCAAAAGCCGA
mUpc5-forward: CTTACTAAAACACGGCTGCAAGTC
mUcp5-reverse: GGCATGAAACATCCCTCTATATTTTAT
mUcp5-son: AAGGCCAGAGTATCGATGTTCGTTTCAAAGA
mGAPDH forward: TGTGTCCGTCGTGGATCTGA
mGAPDH reverse: CCTGCTTCACCACCTTCTTGA
mGAPDH son: CCGCCTGGAGAAACCTGCCAAGTATG

The expression level of UCPs genes was related to GAPDH and presented in relative units using Eq. (1) [25]

$$\sum = 2^{-\Delta ct}, \quad (1)$$

with $\Delta ct = ct(UCP) - ct(GAPDH)$. The threshold cycle (ct) of one sample used for the calculation is a mean value of duplicates.

2.7. Statistical analysis

Data from PCR and Western blot analysis are presented as mean values ± SEM from at least three independent experiments with six to eight specimens for each condition. Data were analyzed with t-test considered statistical significance at $p < 0.05$.

3. Results

3.1. Comparison of UCP2 mRNA and protein expression in CNS of OVA- and MOG-immunized mice at different time points after immunization

To compare the expression levels of different UCPs in the central nervous system (CNS), we subcutaneously injected 6–8 week old female C57BL/6J mice with OVA or MOG.

Because UCP2 is known to be post-translationally regulated [26,27], we performed both WB and PCR to analyze protein (Fig. 1, A-D) and mRNA (Fig. 1, E-F) content at 5, 14 and 21 dpi (days post immunization), which correspond to the pre-clinical stage of EAE, disease peak and decay/chronic stage respectively. We found no UCP2 expression in brain of naïve, OVA and MOG-immunized mice (Fig. 1, A). In SC, UCP2 protein content was increased in OVA- and even more prominent in MOG-immunized animals at 14 dpi in comparison to naïve animals (Fig. 1, B-C). At 21 dpi only MOG-immunized animals showed a slight increase in UCP2 expression (Fig. 1, C). The constant amount of VDAC measured in relation to actin shows that the number of mitochondria did not change during the course of disease (Fig. 1, D). The analysis of gene expression revealed that *ucp2* was not altered in mouse brain at any time point irrespective of the peptide used for immunization (Fig. 1, E). In contrast, *ucp2* in SC was almost five times higher at 14 dpi in MOG-EAE mice as in control mice (Fig. 1, F).

3.2. Comparison of UCP4 expression after EAE induction in SC and brain of MOG/OVA-immunized mice

Because UCP4 is the only UCP we have previously found in neurons, we tested its expression in course of EAE in this work. The quantitative analysis of UCP4 in brain did not reveal differences in protein and gene expression between naïve, OVA- and MOG-immunized mice at all investigated time points after immunization (Fig. 2, A-B), despite a pronounced neuronal disability with high clinical scores (Tabl. 1) and body weight loss (Table 2). Fig. 2 (D-E) demonstrates that UCP4 abundance in SC was decreased at the peak of disease (14 dpi), which we attributed to mitochondria damage, because the expression level of mitochondrial outer membrane protein VDAC was also decreased in SC (Fig. 2, F) in contrast to its expression in brain (Fig. 2, C). No significant changes in UCP4 expression in brain and SC were detected in

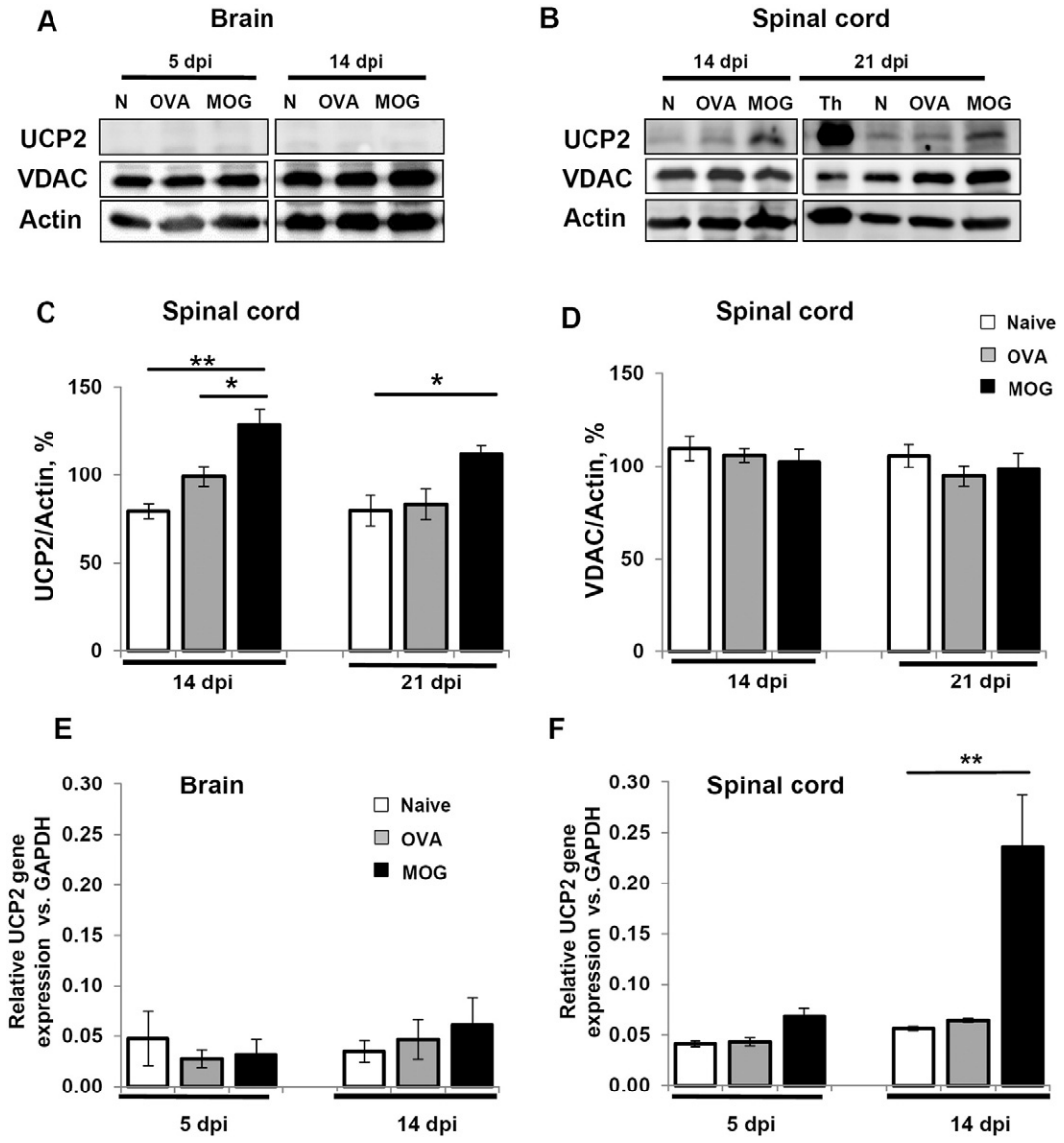

Fig. 1. UCP2 expression in brain and spinal cord of OVA- and MOG-immunized mice. A–B. Representative Western blot images (WB) showing UCP2 expression in brain (A) and spinal cord (B) from naïve (N), OVA- and MOG-immunized animals at 5, 14 and 21 dpi. Anti-VDAC and anti-β-actin antibodies were used as loading controls. For each lane, 20 μg total protein was loaded. C – D. Quantitative analysis of WB images showing the relative distribution of UCP2 (C) and VDAC (D) both normalized to β-actin in spinal cord of naïve (N), OVA and MOG-immunized mice at 14 and 21 dpi. Values represent means ± SEM from four WB with 4–5 animals per each group, $^{*}p < 0.05$; $^{**}p < 0.001$. E–F. UCP2 gene expression analysis performed from whole brain and spinal cord of mice with MOG- and OVA- induced EAE at 5 dpi and 14 dpi. Data are presented as mean ± SEM from five mice per each group, $^{**}p < 0.05$.

OVA-immunized littermates at all investigated time points (Fig. 2, A, B, D, E).

3.3. Visualization of the neuronal mitochondria damage in spinal cord (SC) after MOG/OVA mice immunization

To visualize the neuronal mitochondrial damage we performed a confocal microscopy of SC sections double-immunostained with antibodies against the inner mitochondrial membrane proteins UCP4 and COX (Fig. 3, A), which we evaluated in our previous work [17,28].

Image analysis revealed that the expression pattern of both proteins was altered in MOG-treated mice at 14 dpi. Instead of fine homogeneous distribution of UCP4 that is typical for healthy neurons [18], we detected large conglomerate-like patterns for both proteins, that obviously reflects the changes of mitochondrial morphology in damaged neurons and confirms observations of our and other groups, which described mitochondria swelling in damaged CNS [18,29–32].

The swelling of axonal terminals was reported to not only contain accumulated transport product substances like amyloid precursor proteins (APP) and non-phosphorylated neurofilaments, but also include the injured mitochondria and oxidized phospholipids [33,34]. Using IHC we detected the accumulation of UCP4-positive spheroids in axonal end-bulbs in inflamed lesions of SC at 14 dpi only in MOG-immunized animals (Fig. 3, B). Confocal laser scanning microscopy clearly demonstrated the localization of these spheroids in close vicinity to the activated astrocytes and MHC-class II positive macrophages (Fig. 3, D-E). Single and double IHC with anti-UCP4 antibody and antibody against mitochondrial SOD2 revealed the co-localization of both markers in axonal end-bulbs (Fig. 3, C and F). This finding is in line with data reported by Nikic et al., which demonstrated the accumulation of mitochondria in swelling axonal ends and spheroids in SC of EAE animals [33]. Together these data present the evidence for multiple neuronal damage during EAE progression.

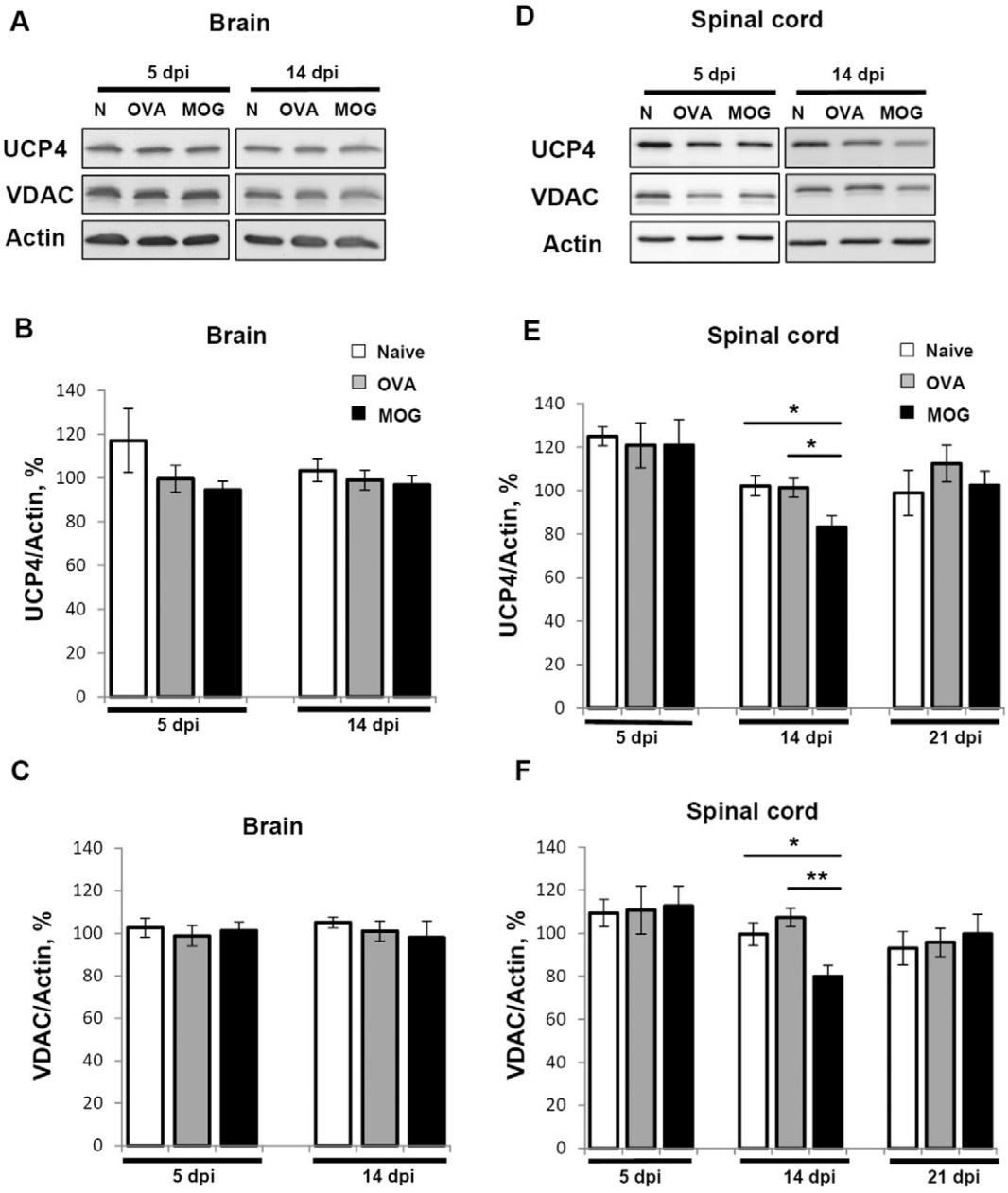

Fig. 2. UCP4 expression in brain and spinal cord of OVA- and MOG-immunized mice. A. Representative Western blot images (WB) showing UCP4 expression in brain of naïve (N), OVA- and MOG-immunized mice at 5 dpi and 14 dpi. VDAC and β-actin were used as controls for mitochondria amount and total protein loading. For each lane, 20 μg protein was loaded. B-C. Quantitative analysis of WB showing the relative UCP4 (B) and VDAC (C) amounts in brain of naïve, control and EAE mice at 5 and 14 dpi. Values represent means ± SEM from eight Western Blots with 6–8 animals per each group. D. Representative WB showing UCP4 expression in spinal cord at 5 dpi and 14 dpi. Anti-VDAC and anti-β-actin were used as controls for mitochondria amount and total protein loading. For each lane, 20 μg protein was loaded. E–F. Quantitative analysis of WBs showing the relative UCP4 (B) and VDAC (C) amounts in spinal cord of naïve, control and EAE mice at 5 and 14 dpi. Values represent means ± SEM from eight WBs with 6–8 animals per each group. *$p < 0.05$; **$p < 0.005$ (Student's T-test).

3.4. UCP5 detection in CNS of naïve, OVA- and MOG-immunized animals

UCP5, originally named as BMCP1 (brain mitochondrial carrier protein 1), was described at mRNA level in brain of human and rodents [35]. We neither detected it in brain nor in SC at protein level under physiological conditions in our previous work [17]. To evaluate whether UCP5 expression was increased under inflammation, we performed a WB analysis using antibodies against UCP5 validated in our previous work and UCP5 recombinant protein as a positive control [17]. Fig. 4, A demonstrates the absence of protein expression in spinal cord of naïve, OVA- and MOG-immunized mice at all investigated time points. In contrast to the results of other investigators [36] we only detected a very low amount of UCP5 at mRNA level (Fig. 4, B-C), that explains the failure of its detection at the protein level as previously discussed [9].

3.5. Investigation of histopathological markers of inflammation up-regulated by EAE

To test at which time points the induction of EAE led to the demyelination and axonal damage typical for EAE-model [37] and to identify the primary cell type responsible for UCP2 up-regulation in SC, we performed a combined staining of SC sections with cell nuclei marker hematoxylin and myelin marker LFB (Fig. 5, A-F) or hematoxylin and T lymphocyte marker CD3 (Fig. 5, G-H). The enhanced lymphocyte

invasion and demyelinated areas in white matter were detected only in SC of MOG-immunized mice at 14 dpi (Fig. 5, F and H). On the protein expression level, the CD3 level was distinctly up-regulated in SC of both groups (OVA- and MOG-immunized mice) at 14 and 21 dpi (Fig. 5, I).

It was previously shown that neurodegeneration caused by MOG immunization strongly correlates with reactive astrogliosis and increased density of microglial cells [21]. In WB we, indeed, detected the elevated levels of IBA1 (Fig. 5, K) and GFAP (Fig. 5, L) immunoreactivity in SC at the peak of disease (14 dpi). To identify the primary cell type responsible for UCP2 up-regulation in SC we investigated the protein expression level of T lymphocyte marker (CD3).

We revealed that the increase of microglial cell density (IBA1-staining, Fig. 6, middle panel) and astrogliosis (GFAP-staining, Fig. 6, low panel) occurred exclusively in SC of MOG-EAE animals and not in OVA-immunized mice. Anti-CD3 staining of SC sections similarly showed the massive T-cells infiltrations of white matter in MOG-immunized mice and to a much less extent in SC of OVA-immunized mice (Fig. 6, upper panel). These findings support our previous data showing the up-regulation of UCP2 in OVA-activated and stimulated T-cells [19]. Thus, we concluded that the up-regulation of UCP2 abundance in SC of immunized animals depends on the presence of activated T-lymphocytes.

3.6. Determination of UCP2 protein content in immune organs of OVA- and MOG-immunized mice

Previously, Vogler et al. [13] observed a decrease of UCP2 mRNA in spleen at day 12 after MOG-immunization. Because thymus microenvironment has been also shown to be affected in acute EAE [38] we investigated a UCP2 protein expression pattern after OVA- and MOG-immunization in thymus and spleen. At 5 dpi, in absence of clinical signs, we did not see any changes in UCP2 content in thymus neither in naïve, nor in OVA- and MOG-immunized mice. A strong decrease of UCP2 levels was detected at all time points in MOG-immunized mice and to a lesser extent in OVA-injected animals in spleen (Fig. 7, C),

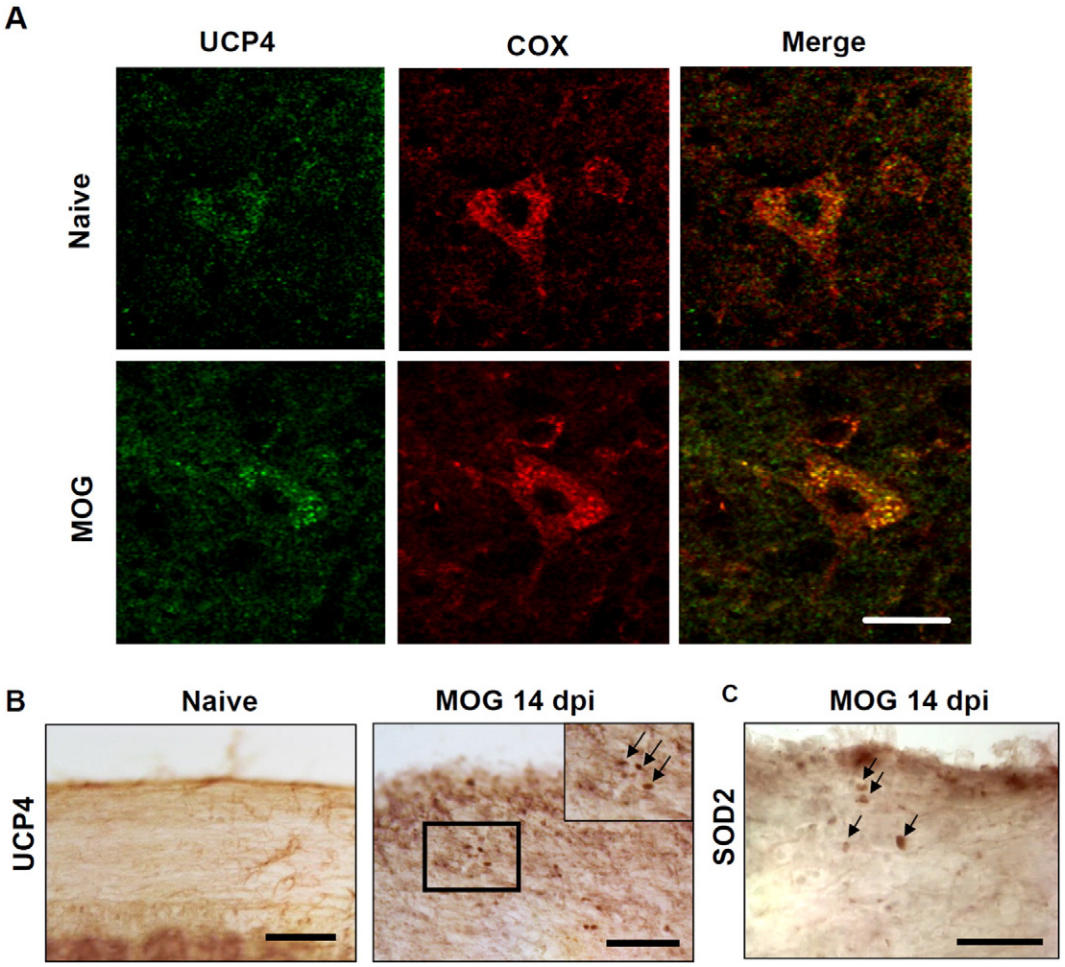

Fig. 3. Visualization of neuronal mitochondria damage in the mouse spinal cord at 14 dpi after MOG-immunization. A. Confocal laser scanning microscopy image of motor neurons in lumbar spinal cord. Neurons were immunostained with anti-COX (visualized by Alexa 568, red) and anti-UCP4 (visualized by Alexa 488, green) in naïve (upper row) and MOG (lower row) immunized mouse. Immunostaining was performed on 50 μm thick longitudinal vibratome sections of fixed spinal cord. Scale bar, 10 μm. B–C. Representative images demonstrating the expression of UCP4 (B) and SOD2 (C) in white matter of longitudinal sections of spinal cord from naïve and MOG-immunized mice at 14 dpi. Staining with primary antibodies were amplified by ABC and visualized with DAB. Immunostaining was performed on 50 μm thick longitudinal vibratome sections of spinal cord. Scale bar, 30 μm. D. Confocal laser scanning microscopy image of lesion in white matter of spinal cord. Double-immunostaining was performed with anti-GFAP (visualized by Alexa 568, red) and anti-UCP4 (visualized by Alexa 488, green). UCP4-positive axonal spheroids were detected in close vicinity of activated astrocytes. Immunostaining was performed on 50 μm thick longitudinal vibratome sections of spinal cord. Scale bar, 20 μm. E. Confocal laser scanning microscopy images show the localization of UCP4-positive spheroids (visualized by Alexa 488, green) near the MHC-class II-positive (visualized by Alexa 568, red) cells in inflammatory lesion of the white matter of spinal cord. Immunostaining was performed on 50 μm thick longitudinal vibratome sections of spinal cord. Scale bar, 20 μm. F. Confocal laser scanning microscopy shows the co-localization of UCP4 (green) and SOD2 (red) in spheroids and axonal bulbs in a inflammatory lesion of spinal cord. Double-labeling with anti-UCP4 antibody (Alexa-488, green) and anti-SOD2 (Alexa-568, red) antibodies was performed on 20 μm thick cryostat sections. Scale bar, 10 μm.

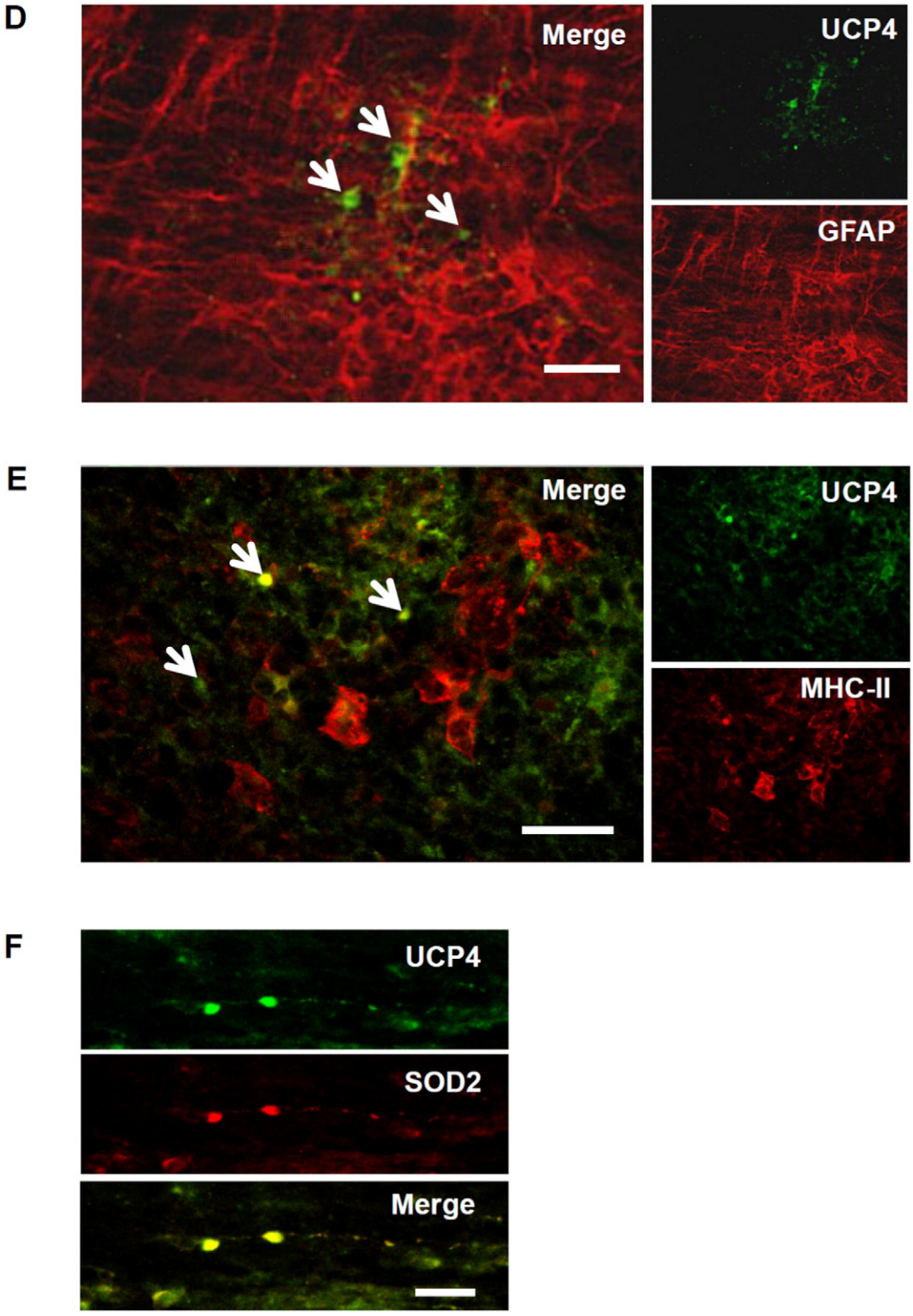

Fig. 3 (*continued*).

whereas UCP2 decrease in thymus was more moderate at 14 dpi (Fig. 7, A). Three weeks after immunization (21 dpi), we observed even an increase of UCP2 expression in the thymus of both OVA- and MOG-groups (Fig. 7, A).

Interestingly, the alteration of the UCP2 expression pattern coincided with the CD3 expression profile (Fig. 7, B). Notably, the immunization with OVA- and MOG-peptides led to a stable decrease in CD3 levels at all investigated time-points in the spleen (Fig 7, D). At 14 and 21 dpi we detected a pronounced up-regulation of the mitochondrial stress marker Hsp60, probably due to activation of IBA1-positive macrophages and epithelial cells in thymus and spleen of OVA- and MOG-immunized animals (Fig. 7, B and D). Thus, our data demonstrated

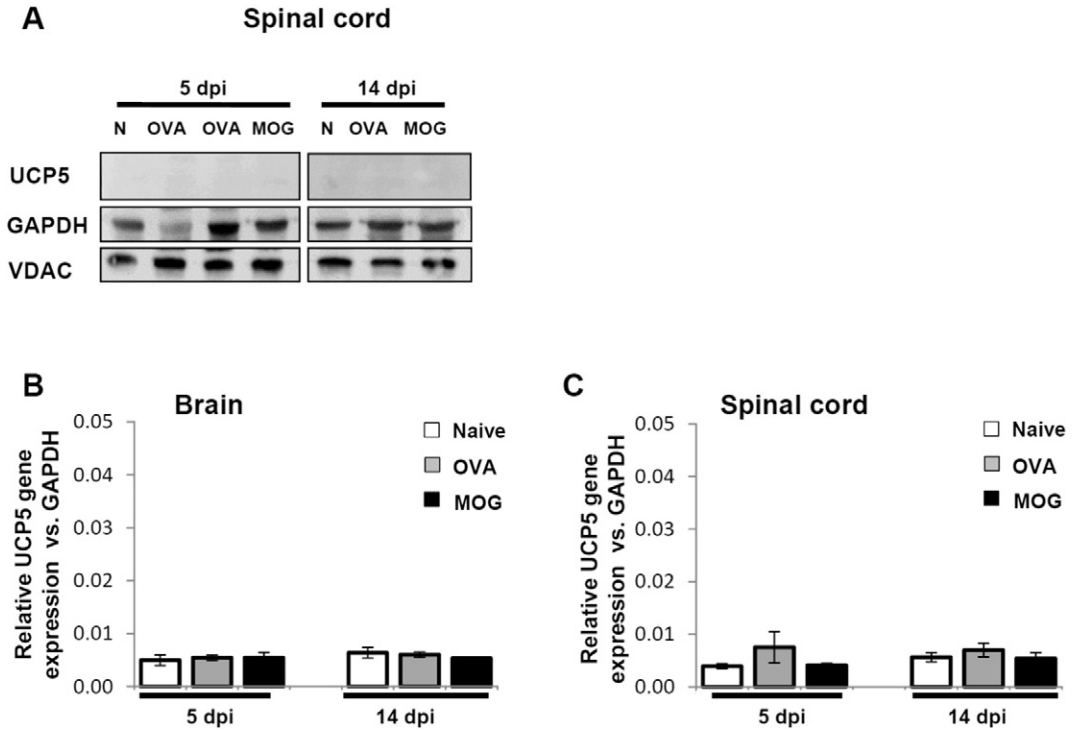

Fig. 4. UCP5 expression in brain and spinal cord of OVA- and MOG-immunized mice. A. Representative Western blot images of protein extracts from spinal cord of naïve (N), OVA- and MOG-immunized animals at 5 and 14 dpi immunostained with anti-UCP5, anti-VDAC and anti-GAPDH antibodies. For each lane, 20 μg protein was loaded. B-C. UCP5 gene expression analysis in whole brain (B) and spinal cord (C) of mice with active EAE, induced by MOG or by OVA at day 5 or 14 dpi. Values represent a mean ± SEM of four mice per each group.

the participation of thymus and spleen in EAE progression, and showed that the UCP2 protein content in these immune organs is directly associated with the expansion of the CD3-positive T-cell population.

4.. Discussion

In the present study we demonstrated that the up-regulation of UCP2 expression after EAE induction (i) occurred only in spinal cord, (ii) directly correlated with the time-course of EAE being the highest at the peak of the disease (14 dpi), (iii) was antigen-independent, i.e. could be induced both by non-specific OVA and EAE-specific MOG immunization, and (iv) coincided with the alteration of $CD3^+$ T-lymphocyte amount during immune response. Therefore, our data partly support the previous studies demonstrating the elevation of *ucp2* gene level in SC during the course of active induced EAE [13,16]. In view of our recent data that shows the absence of UCP2 in neurons [19], we hypothesized that the possible cause for UCP2 expression changes can be linked to the common activation of the immune cells due to inflammation. It is known, that the initiation of disease and extent of neuronal damage during the course of EAE is associated with the infiltration of CNS parenchyma by myelin-specific T-cells [39]. Because no immunohistological evidence for the UCP2 up-regulation in these cells can be obtained due to poor antibody performance, we evaluated the time course of expression of several cell markers for T-lymphocytes, macrophages and astrocytes and paralleled it to the time course of UCP2 expression during EAE. The results revealed that the up-regulation of UCP2 level corresponded to the peak of acute and chronic phases of EAE and correlated with the massive infiltration of activated encephalitogenic T-cells shown by anti-CD3 antibody immunostaining. Further evidence which links UCP2 expression to the invasion of activated lymphocytes is the moderate up-regulation of UCP2 protein level in SC by animal immunization with a CNS-irrelevant antigen ovalbumin (OVA) [40]. The current observations confirm our previous data showing that non-CNS-specific T-lymphocytes transmigrate the brain blood barrier and penetrate CNS parenchyma without promoting neuropathology [21]. In contrast to MOG-stimulated T-cells, the lymphocytes from OVA-immunized animals were not able to encounter their antigen in SC parenchyma for re-stimulation and for persisting in CNS during long time periods [41]. Indeed, the selective up-regulation of mitochondrial UCP2 levels in stimulated OT-II T-lymphocytes was detected only after specific re-stimulation [19], that probably occurred due to the intensive production of cytokines and an increase of glutamine uptake [42,43]. An additional supporting fact for this suggestion is the simultaneous down-regulation of the CD3-marker and UCP2 in immune organs at 14 dpi after immunization with both OVA and MOG peptides. This finding indirectly confirms the data from a previous study [38], which revealed first morphological alterations in rat thymus around 12 dpi after EAE induction. Moreover, the ultra-structural and morphological observations at this time-point show depletion of thymocytes from the thymus and an enlargement of intercellular volumes which can be due to T-lymphocyte movement from the thymus into the blood vessels. The decrease of the UCP2 mRNA level in spleen at day 12 after MOG-immunization was also described by Vogler and colleagues [13].

In contrast to MOG-immunized animals, the UCP2 expression level in SC of OVA-immunized mice was not prominent. CNS infiltration by MOG-specific T-cells induced the astro- and microgliosis – characteristic hallmarks of neuroinflammation during MS and EAE – confirming the results of other groups [44,45]. Indeed, we observed the IBA1- and GFAP-immune-positivity only in SC of MOG-immunized mice (Fig. 5, K-L), which is in line with our previous reports [21,46]. Taken into account that UCP2 was detected in macrophages [47] and in microglia [19], we postulate that mitochondria from microglial cells could also partly be responsible for the elevation of the UCP2 protein level in the SC of MOG immunized mice on 14 and 21 dpi.

5. Conclusion

In this work we used EAE, the animal model of MS, and self-designed anti-UCP antibodies, which we have evaluated in our previous work. To get a deeper insight into the molecular mechanisms, we not only

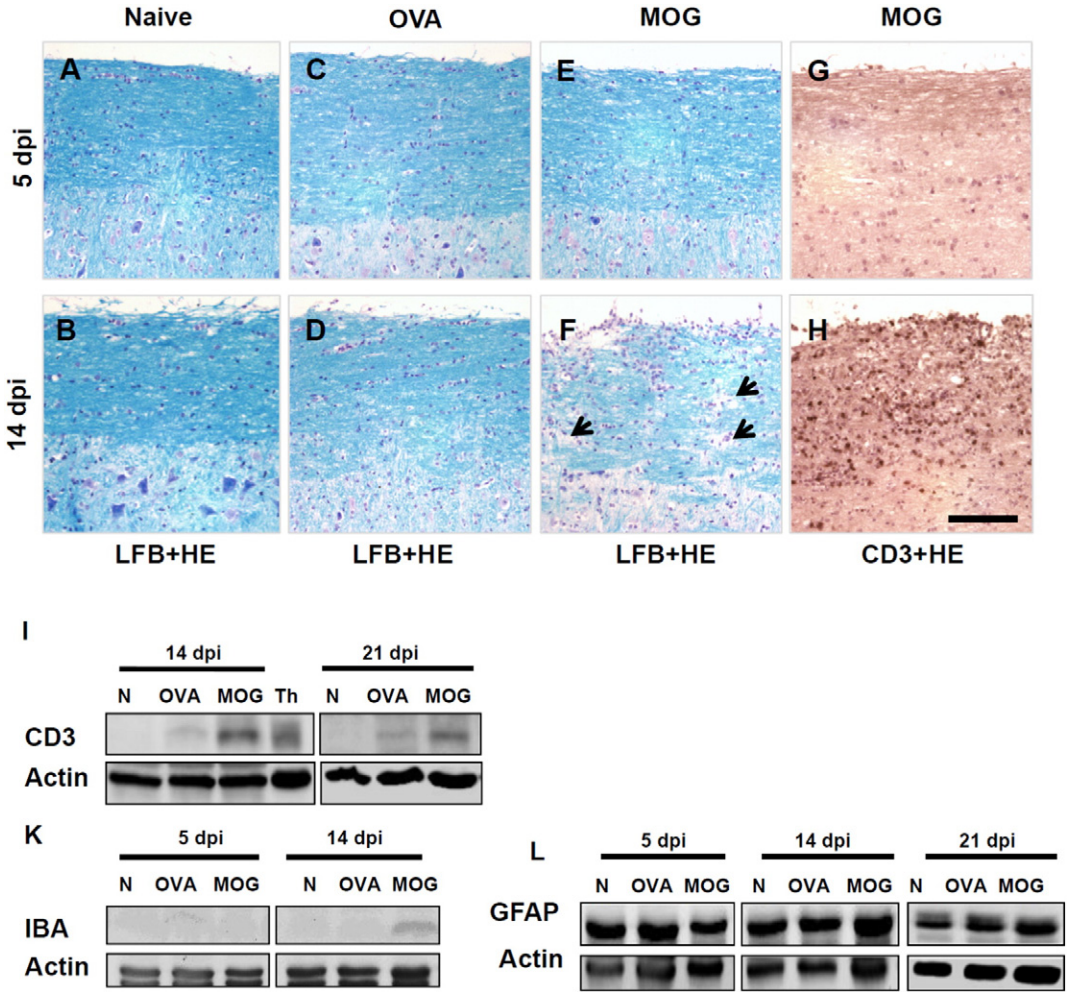

Fig. 5. Investigation of inflammation markers up-regulated by EAE. (A–H) Histopathological analyses of the longitudinal spinal cord sections from OVA and MOG-immunized mice in preclinical phase (5 dpi) and at the peak of EAE (14 dpi). Simultaneous Luxol Fast Blue (LFB) and hematoxyline staining (A–F) indicates the white matter demyelination in close vicinity to cell infiltration in spinal cord of MOG-EAE mice (F, arrows). Anti-CD3 immunohistochemistry (G–H) detected massive accumulation of activated T-cells (anti-$CD3^+$ staining) in spinal cord of MOG-immunized animals at 14 dpi (H). Immunostaining was performed on 8 μm thick longitudinal paraffin embedded sections of spinal cord. Scale bar corresponds to 50 μm and applies to all images. I–L. Representative Western blot images of spinal cord lysates from naïve (N), OVA- and MOG-immunized animals immunostained with anti-CD3 (I), anti-IBA1 (K) and anti-GFAP (L). For each lane, 100 μg (I) or 50 μg (K–L) protein was loaded. Anti-β-actin antibody was used as a loading control.

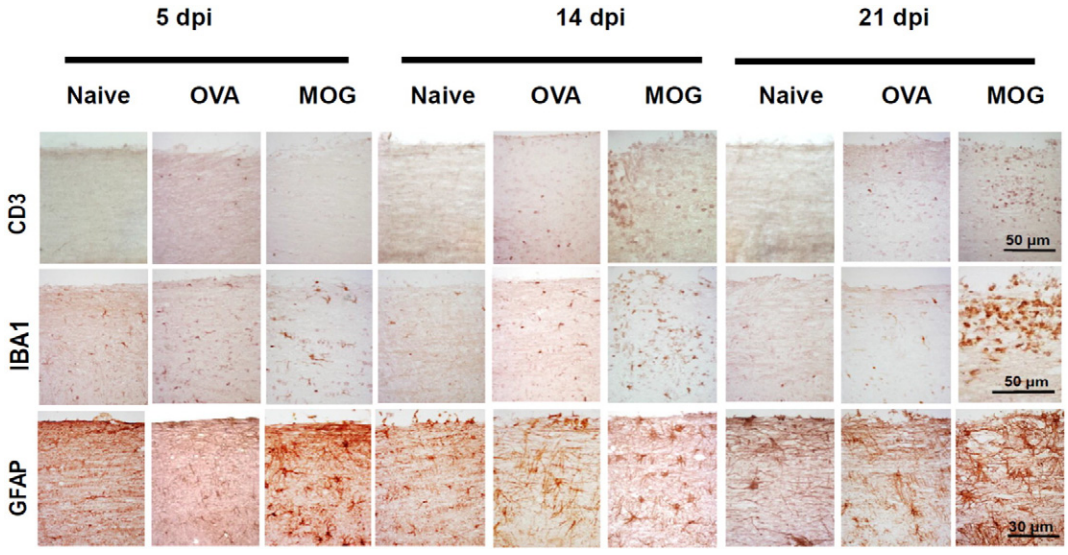

Fig. 6. Visualization of T-lymphocytes ($CD3^+$-positive), activated microglia (IBA1-positive) and astrocytes (GFAP-positive) in spinal cord of naïve, OVA- and MOG-immunized mice. DAB-Immunostaining was performed on 8 μm thick longitudinal paraffin embedded sections of spinal cord.

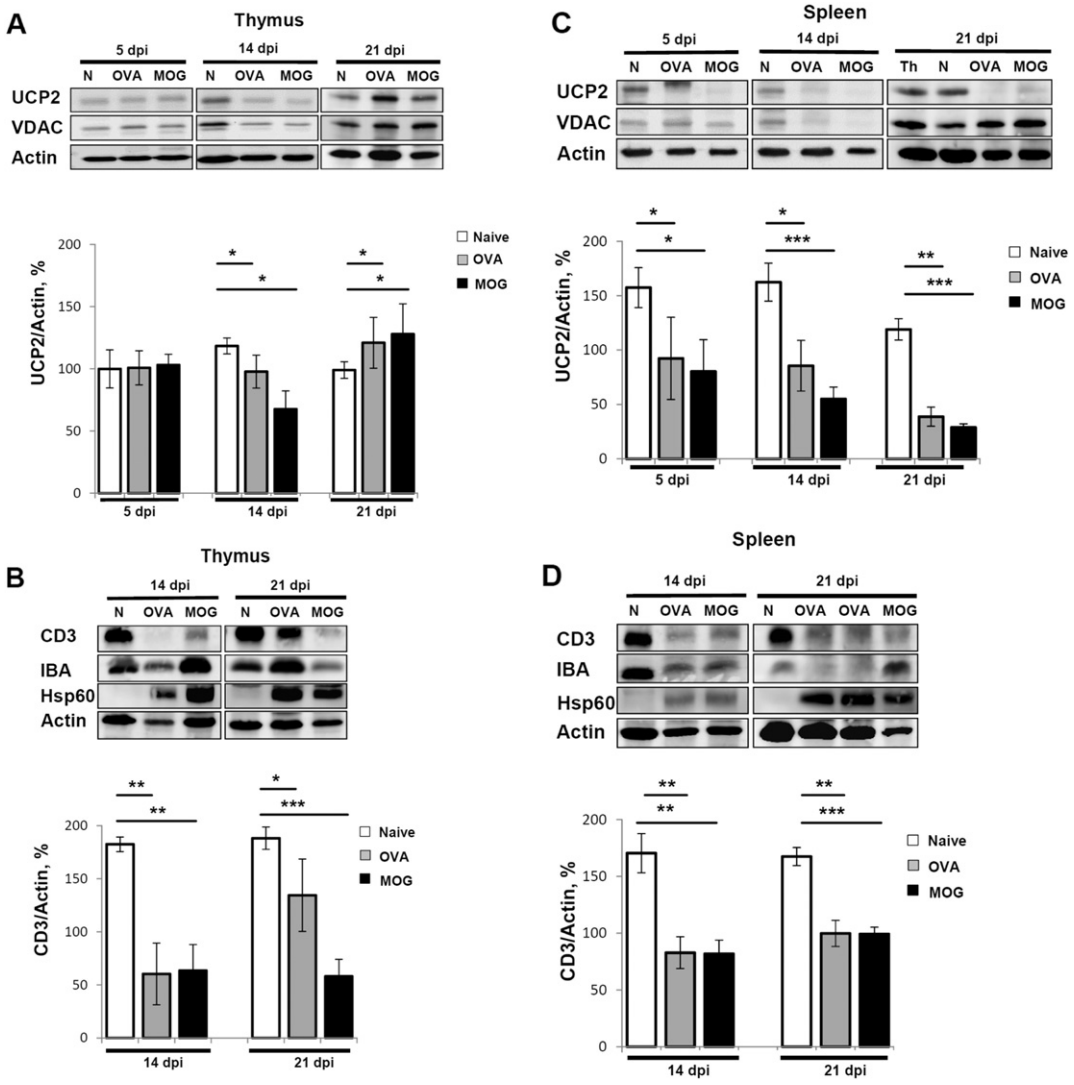

Fig. 7. UCP2 expression in thymus and spleen of OVA- and MOG-immunized mice. Representative WB images and UCP2/CD3 quantification of thymus (A-B) and spleen (C-D) from naïve (N), OVA- and MOG-immunized animals immunostained with anti-UCP2, anti-IBA1, anti-CD3, anti-Hsp60 antibodies. Anti-VDAC and anti-β-actin antibodies were used as loading control. For each lane 50 μg protein was loaded. Data are presented as mean ± SEM of 3–5 mice per group; *p < 0.5, **p < 0.01, ***p < 0.001.

investigated the expression of UCP2, UCP4 and UCP5 at different EAE stages in brain and spinal cord, but also compared it to UCP expression after unspecific activation of immune system by ovalbumin. We show for the first time that the abundance of UCP4, which is only present in neurons, is not affected within the course time of disease. For a long time it had been supposed that the activity of UCP2 in neurons would regulate the proton gradient and therefore the production of ROS. Our current results demonstrated that UCP2 is not present in neurons under neuroinflammatory conditions. In contrast, we have correlated the elevated amounts of UCP2 in spinal cord with the lymphocyte invasion, released by EAE-specific MOG antigen. Our results clearly indicate that of the three different UCPs, only UCP2 in specifically activated lymphocytes may represent a potential target for MS treatment.

Conflict of interest

The authors declare no conflict of interest.

Transparency document

The Transparency document associated with this article can be found in the online version.

Acknowledgments

EP and AR are grateful to BMBS COST Action BM1406 (IONCHAN-IMMUNRESPON) for the scientific exchange and cooperation. We thank Marion Langer and Christian Pazmandi (Institute of Physiology, Pathophysiology and Biophysics, University of Veterinary Medicine, Vienna, Austria) for the help with mice handling. We thank Quentina Beatty for editorial assistance as a native English speaker.

References

[1] V. Siffrin, J. Vogt, H. Radbruch, R. Nitsch, F. Zipp, Multiple sclerosis — candidate mechanisms underlying CNS atrophy, Trends Neurosci. 33 (2010) 202–210.
[2] H. Lassmann, Pathology and disease mechanisms in different stages of multiple sclerosis, J. Neurol. Sci. 333 (2013) 1–4.
[3] M.T. Fischer, R. Sharma, J.L. Lim, L. Haider, J.M. Frischer, J. Drexhage, D. Mahad, M. Bradl, H.J. Van, H. Lassmann, NADPH oxidase expression in active multiple sclerosis lesions in relation to oxidative tissue damage and mitochondrial injury, Brain 135 (2012) 886–899.
[4] M.E. Witte, D.J. Mahad, H. Lassmann, H.J. Van, Mitochondrial dysfunction contributes to neurodegeneration in multiple sclerosis, Trends Mol. Med. 20 (2014) 179–187.
[5] H.J. Van, M.E. Witte, G. Schreibelt, H.E. de Vries, Radical changes in multiple sclerosis pathogenesis, Biochim. Biophys. Acta 1812 (2011) 141–150.
[6] Y. Gilgun-Sherki, E. Melamed, D. Offen, The role of oxidative stress in the pathogenesis of multiple sclerosis: the need for effective antioxidant therapy, J. Neurol. 251 (2004) 261–268.

[7] V.P. Skulachev, Uncoupling: new approaches to an old problem of bioenergetics, Biochim. Biophys. Acta 1363 (1998) 100–124.
[8] S. Krauss, C.Y. Zhang, B.B. Lowell, The mitochondrial uncoupling-protein homologues, Nat. Rev. Mol. Cell Biol. 6 (2005) 248–261.
[9] A. Rupprecht, D. Sittner, A. Smorodchenko, K.E. Hilse, J. Goyn, R. Moldzio, A.E. Seiler, A.U. Brauer, E.E. Pohl, Uncoupling protein 2 and 4 expression pattern during stem cell differentiation provides new Insight into their putative function, PLoS ONE 9 (2014) e88474.
[10] C. Pecqueur, C. Alves-Guerra, D. Ricquier, F. Bouillaud, UCP2, a metabolic sensor coupling glucose oxidation to mitochondrial metabolism? IUBMB Life 61 (2009) 762–767.
[11] H.E. Andrews, P.P. Nichols, D. Bates, D.M. Turnbull, Mitochondrial dysfunction plays a key role in progressive axonal loss in multiple sclerosis, Med. Hypotheses 64 (2005) 669–677.
[12] S. Vogler, R. Goedde, B. Miterski, R. Gold, A. Kroner, D. Koczan, U.K. Zettl, P. Rieckmann, J.T. Epplen, S.M. Ibrahim, Association of a common polymorphism in the promoter of UCP2 with susceptibility to multiple sclerosis, J. Mol. Med. 83 (2005) 806–811.
[13] S. Vogler, J. Pahnke, S. Rousset, D. Ricquier, H. Moch, B. Miroux, S.M. Ibrahim, Uncoupling protein 2 has protective function during experimental autoimmune encephalomyelitis, Am. J. Pathol. 168 (2006) 1570–1575.
[14] C. Aheng, N. Ly, M. Kelly, S. Ibrahim, D. Ricquier, M.C. Alves-Guerra, B. Miroux, Deletion of UCP2 in iNOS deficient mice reduces the severity of the disease during experimental autoimmune encephalomyelitis, PLoS ONE 6 (2011) e22841.
[15] D. Otaegui, A. Saenz, J. Ruiz-Martinez, J. Olaskoaga, A. Lopez de Munain, UCP2 and mitochondrial haplogroups as a multiple sclerosis risk factor, Mult. Scler. 13 (2007) 454–458.
[16] S.M. Ibrahim, E. Mix, T. Bottcher, D. Koczan, R. Gold, A. Rolfs, H.J. Thiesen, Gene expression profiling of the nervous system in murine experimental autoimmune encephalomyelitis, Brain 124 (2001) 1927–1938.
[17] A. Smorodchenko, A. Rupprecht, I. Sarilova, O. Ninnemann, A.U. Brauer, K. Franke, S. Schumacher, S. Techritz, R. Nitsch, M. Schuelke, E.E. Pohl, Comparative analysis of uncoupling protein 4 distribution in various tissues under physiological conditions and during development, Biochim. Biophys. Acta 1788 (2009) 2309–2319.
[18] A. Smorodchenko, A. Rupprecht, J. Fuchs, J. Gross, E.E. Pohl, Role of mitochondrial uncoupling protein 4 in rat inner ear, Mol. Cell. Neurosci. 47 (2011) 244–253.
[19] A. Rupprecht, A.U. Brauer, A. Smorodchenko, J. Goyn, K.E. Hilse, I.G. Shabalina, C. Infante-Duarte, E.E. Pohl, Quantification of uncoupling protein 2 reveals its main expression in immune cells and selective up-regulation during T-cell proliferation, PLoS ONE 7 (2012) e41406.
[20] S. Rousset, Y. Emre, O. Join-Lambert, C. Hurtaud, D. Ricquier, A.M. Cassard-Doulcier, The uncoupling protein 2 modulates the cytokine balance in innate immunity, Cytokine 35 (2006) 135–142.
[21] A. Smorodchenko, J. Wuerfel, E.E. Pohl, J. Vogt, E. Tysiak, R. Glumm, S. Hendrix, R. Nitsch, F. Zipp, C. Infante-Duarte, CNS-irrelevant T-cells enter the brain, cause blood–brain barrier disruption but no glial pathology, Eur. J. Neurosci. 26 (2007) 1387–1398.
[22] H. Kluver, E. Barrera, A method for the combined staining of cells and fibers in the nervous system, J. Neuropathol. Exp. Neurol. 12 (1953) 400–403.
[23] V. Beck, M. Jaburek, T. Demina, A. Rupprecht, R.K. Porter, P. Jezek, E.E. Pohl, Polyunsaturated fatty acids activate human uncoupling proteins 1 and 2 in planar lipid bilayers, FASEB J. 21 (2007) 1137–1144.
[24] K.E. Hilse, A.V. Kalinovich, A. Rupprecht, A. Smorodchenko, U. Zeitz, K. Staniek, R.G. Erben, E.E. Pohl, The expression of UCP3 directly correlates to UCP1 abundance in brown adipose tissue, Biochim. Biophys. Acta 1857 (2016) 72–78.
[25] K.J. Livak, T.D. Schmittgen, Analysis of relative gene expression data using real-time quantitative PCR and the 2(-Delta Delta C(T)) method, Methods 25 (2001) 402–408.
[26] C. Pecqueur, M.C. Alves-Guerra, C. Gelly, C. Levi-Meyrueis, E. Couplan, S. Collins, D. Ricquier, F. Bouillaud, B. Miroux, Uncoupling protein 2, in vivo distribution, induction upon oxidative stress, and evidence for translational regulation, J. Biol. Chem. 276 (2001) 8705–8712.
[27] C. Hurtaud, C. Gelly, F. Bouillaud, C. Levi-Meyrueis, Translation control of UCP2 synthesis by the upstream open reading frame, Cell. Mol. Life Sci. 63 (2006) 1780–1789.
[28] E. Klotzsch, A. Smorodchenko, L. Löfler, R. Moldzio, E. Parkinson, G.J. Schütz, E.E. Pohl, Superresolution microscopy reveals spatial separation of UCP4 and F(0)F(1)-ATP synthase in neuronal mitochondria, Proc. Natl. Acad. Sci. U. S. A. 112 (2015) 130–135.
[29] Y. Kageyama, Z. Zhang, R. Roda, M. Fukaya, J. Wakabayashi, N. Wakabayashi, T.W. Kensler, P.H. Reddy, M. Iijima, H. Sesaki, Mitochondrial division ensures the survival of postmitotic neurons by suppressing oxidative damage, J. Cell Biol. 197 (2012) 535–551.
[30] U. Schulze-Topphoff, A. Prat, T. Prozorovski, V. Siffrin, M. Paterka, J. Herz, I. Bendix, I. Ifergan, I. Schadock, M.A. Mori, H.J. Van, F. Schroter, A. Smorodchenko, M.H. Han, M. Bader, L. Steinman, O. Aktas, F. Zipp, Activation of kinin receptor B1 limits encephalitogenic T lymphocyte recruitment to the central nervous system, Nat. Med. 15 (2009) 788–793.
[31] B. Ferguson, M.K. Matyszak, M.M. Esiri, V.H. Perry, Axonal damage in acute multiple sclerosis lesions, Brain 120 (Pt 3) (1997) 393–399.
[32] B.D. Trapp, K.A. Nave, Multiple sclerosis: an immune or neurodegenerative disorder? Annu. Rev. Neurosci. 31 (2008) 247–269.
[33] I. Nikic, D. Merkler, C. Sorbara, M. Brinkoetter, M. Kreutzfeldt, F.M. Bareyre, W. Bruck, D. Bishop, T. Misgeld, M. Kerschensteiner, A reversible form of axon damage in experimental autoimmune encephalomyelitis and multiple sclerosis, Nat. Med. 17 (2011) 495–499.
[34] L. Haider, M.T. Fischer, J.M. Frischer, J. Bauer, R. Hoftberger, G. Botond, H. Esterbauer, C.J. Binder, J.L. Witztum, H. Lassmann, Oxidative damage in multiple sclerosis lesions, Brain 134 (2011) 1914–1924.
[35] D. Sanchis, C. Fleury, N. Chomiki, M. Goubern, Q. Huang, M. Neverova, F. Gregoire, J. Easlick, S. Raimbault, C. Levi-Meyrueis, B. Miroux, S. Collins, M. Seldin, D. Richard, C. Warden, F. Bouillaud, D. Ricquier, BMCP1, a novel mitochondrial carrier with high expression in the central nervous system of humans and rodents, and respiration uncoupling activity in recombinant yeast, J. Biol. Chem. 273 (1998) 34611–34615.
[36] M.E. Witte, P.G. Nijland, J.A. Drexhage, W. Gerritsen, D. Geerts, H.B. van Het, A. Reijerkerk, H.E. de Vries, Valk Van der, H.J. Van, Reduced expression of PGC-1alpha partly underlies mitochondrial changes and correlates with neuronal loss in multiple sclerosis cortex, Acta Neuropathol. 125 (2013) 231–243.
[37] O. Aktas, A. Smorodchenko, S. Brocke, C. Infante-Duarte, U.S. Topphoff, J. Vogt, T. Prozorovski, S. Meier, V. Osmanova, E. Pohl, I. Bechmann, R. Nitsch, F. Zipp, Neuronal damage in autoimmune neuroinflammation mediated by the death ligand TRAIL, Neuron 46 (2005) 421–432.
[38] D. Cavallotti, V. D'Andrea, F.S. Pastore, F.M. Leali, C. Cavallotti, Pathogenesis of some neurological immune ultrastructural and morphometrical observations on rat thymus, Neurol. Res. 27 (2005) 41–46.
[39] S. Kuerten, P.V. Lehmann, The immune pathogenesis of experimental autoimmune encephalomyelitis: lessons learned for multiple sclerosis? J. Interf. Cytokine Res. 31 (2011) 907–916.
[40] J.A. Huntington, P.E. Stein, Structure and properties of ovalbumin 16, J. Chromatogr. B Biomed. Sci. Appl. 756 (2001) 189–198.
[41] N. Kawakami, F. Odoardi, T. Ziemssen, M. Bradl, T. Ritter, O. Neuhaus, H. Lassmann, H. Wekerle, A. Flugel, Autoimmune CD4 + T cell memory: lifelong persistence of encephalitogenic T cell clones in healthy immune repertoires, J. Immunol. 175 (2005) 69–81.
[42] H. Cortez-Pinto, S.Q. Yang, H.Z. Lin, S. Costa, C.S. Hwang, M.D. Lane, G. Bagby, A.M. Diehl, Bacterial lipopolysaccharide induces uncoupling protein-2 expression in hepatocytes by a tumor necrosis factor-alpha-dependent mechanism, Biochem. Biophys. Res. Commun. 251 (1998) 313–319.
[43] Y. Emre, T. Nubel, Uncoupling protein UCP2: when mitochondrial activity meets immunity, FEBS Lett. 584 (2010) 1437–1442.
[44] F. Zipp, O. Aktas, The brain as a target of inflammation: common pathways link inflammatory and neurodegenerative diseases, Trends Neurosci. 29 (2006) 518–527.
[45] L.K. Peterson, R.S. Fujinami, Inflammation, demyelination, neurodegeneration and neuroprotection in the pathogenesis of multiple sclerosis, J. Neuroimmunol. 184 (2007) 37–44.
[46] J. Vogt, F. Paul, O. Aktas, K. Muller-Wielsch, J. Dorr, S. Dorr, B.S. Bharathi, R. Glumm, C. Schmitz, H. Steinbusch, C.S. Raine, M. Tsokos, R. Nitsch, F. Zipp, Lower motor neuron loss in multiple sclerosis and experimental autoimmune encephalomyelitis, Ann. Neurol. 66 (2009) 310–322.
[47] C. Fleury, M. Neverova, S. Collins, S. Raimbault, O. Champigny, C. Levi-Meyrueis, F. Bouillaud, M.F. Seldin, R.S. Surwit, D. Ricquier, C.H. Warden, Uncoupling protein-2: a novel gene linked to obesity and hyperinsulinemia, Nat. Genet. 15 (1997) 269–272.